Biochemical Journal (2023) **480** 1805–1816
https://doi.org/10.1042/BCJ20230384

Research Article

Loss of the methylarginine reader function of SND1 confers resistance to hepatocellular carcinoma

Tanner Wright[1,2,*], Yalong Wang[1,*], Sabrina A. Stratton[1], Manu Sebastian[3], Bin Liu[1], David G. Johnson[1] and Mark T. Bedford[1]

[1]Department of Epigenetics and Molecular Carcinogenesis, The University of Texas MD Anderson Cancer Center, Houston, TX 77030, U.S.A.; [2]MD Anderson UTHealth Houston, Graduate School of Biomedical Sciences, 6767 Bertner Ave, Houston, TX 77030, U.S.A.; [3]Department of Veterinary Medicine and Surgery, The University of Texas MD Anderson Cancer Center, Houston, TX 77030, U.S.A.

Correspondence: Mark T. Bedford (mtbedford@mdanderson.org)

Staphylococcal nuclease Tudor domain containing 1 (SND1) protein is an oncogene that 'reads' methylarginine marks through its Tudor domain. Specifically, it recognizes methylation marks deposited by protein arginine methyltransferase 5 (PRMT5), which is also known to promote tumorigenesis. Although SND1 can drive hepatocellular carcinoma (HCC), it is unclear whether the SND1 Tudor domain is needed to promote HCC. We sought to identify the biological role of the SND1 Tudor domain in normal and tumorigenic settings by developing two genetically engineered SND1 mouse models, an *Snd1* knockout (*Snd1 KO*) and an *Snd1* Tudor domain-mutated (*Snd1 KI*) mouse, whose mutant SND1 can no longer recognize PRMT5-catalyzed methylarginine marks. Quantitative PCR analysis of normal, KO, and KI liver samples revealed a role for the SND1 Tudor domain in regulating the expression of genes encoding major acute phase proteins, which could provide mechanistic insight into SND1 function in a tumor setting. Prior studies indicated that ectopic overexpression of SND1 in the mouse liver dramatically accelerates the development of diethylnitrosamine (DEN)-induced HCC. Thus, we tested the combined effects of DEN and SND1 loss or mutation on the development of HCC. We found that both *Snd1 KO* and *Snd1 KI* mice were partially protected against malignant tumor development following exposure to DEN. These results support the development of small molecule inhibitors that target the SND1 Tudor domain or the use of upstream PRMT5 inhibitors, as novel treatments for HCC.

Introduction

Arginine methylation is an abundant posttranslational modification (PTM) that occurs in three forms in mammals: asymmetric dimethylarginine (ADMA), symmetric dimethylarginine (SDMA) and monomethylarginine (MMA) [1]. These distinct methyl marks are deposited by different protein arginine methyltransferases (PRMTs), a family which comprises nine members, including PRMT5 that deposits the majority of SDMA marks [2]. Arginine methylation of a protein substrate can impact that protein's function in several ways. It can: (1) regulate nuclear/cytoplasmic shuttling of proteins; (2) modulate PTM deposition of kinase substrates when in proximity to phosphorylation sites; and (3) generate docking sites for effector proteins that relay signaling information through the cell. These effector proteins typically harbor Tudor domains that 'read' the methylation motifs [3].

One such reader or 'effector' protein that recognizes PRMT5-catalyzed SDMA marks is Staphylococcal nuclease domain-containing protein 1 (SND1). SND1 harbors four tandem Staphylococcal nuclease like (SN) domains and a C-terminal Tudor domain that interrupts a fifth SN domain [4]. SND1 is also referred to as p100, TSN and TDRD11, and is enriched for in secretory tissues like the liver and pancreas [5]. Structure studies of the SND1 Tudor domain reveal that it binds SDMA marks through an aromatic cage [6,7]. The SND1 Tudor domain directly interacts with

*These authors contributed equally to this work.

Received: 12 September 2023
Revised: 30 October 2023
Accepted: 31 October 2023

Accepted Manuscript online: 31 October 2023
Version of Record published: 17 November 2023

Biochemical Journal (2023) **480** 1805–1816
https://doi.org/10.1042/BCJ20230384

arginine methylated forms of glycine-arginine-rich (GAR) motifs in splicing factors including SmB/B', SmD1, SmD3, and Sam68 [8,9]. It also binds directly to a SDMA motif in the E2F1 transcription factor [10] and modulates the splicing of a subset of E2F1 transcriptional target genes [11]. SND1 is a transcriptional coactivator for Epstein–Barr virus nuclear antigen 2 (EBNA-2) [12] and for signal transducer and activator of transcription 5 and 6 (STAT5 and STAT6) [13,14]. Furthermore, argonaute RISC catalytic component 2 (AGO2) is methylated by PRMT5, to create a docking motif for SND1 [15]. Thus, this SDMA effector protein has a number of methyl-dependent binding partners that are implicated in transcriptional regulation and RNA processing.

SND1 acts as an oncogene in a number of different cancer settings [4,16], particularly as a molecular driver of hepatocellular carcinoma (HCC) [5,17]. *SND1* is up-regulated in several cancers and is positively correlated with worse disease prognosis [18]. Immunostaining of a tissue microarray showed that 74% of patient HCC samples overexpressed SND1 [19]. Furthermore, mutagenic Sleeping Beauty transposon screens in mice revealed *Snd1* as a potential driver of HCC in both *Pten* null and chronic hepatitis B mouse models [20,21]. However, the most direct evidence for *Snd1* as an oncogene in HCC was generated using a genetically engineered mouse model (GEMM) that overexpressed SND1 in the liver resulting in spontaneous carcinoma and an exacerbated tumorigenic response when combined with carcinogen-induced HCC [22].

The contribution of the SND1 Tudor domain to the oncogenic activity of SND1 is unknown. Virtually all SDMA in the cell is deposited by PRMT5, an enzyme which also has oncogenic properties [23–25]. Interest in PRMT5 as a therapeutic target is expanding, in part, because of the recent development of increasingly effective small molecule inhibitors of PRMT5 [23,26,27]. Given the relationship between the putative oncogenic roles of PRMT5 and SND1, especially that the SND1 Tudor domain reads SDMA marks, we developed a GEMM to facilitate the structure/function analysis of SND1 *in vivo*. *Snd1* knockout mouse models have recently been developed by two independent groups [28,29]. Both groups generated conditional knockout mice but used systemic knockouts for their studies, as the *Snd1* null mice were viable. They showed that SND1 plays a role in the immune response against bacterial infection [28], and that SND1 regulates the expression of major acute phase proteins (APPs) in the liver that are involved in innate immunity [29]. These full knockouts of SND1 remove all SND1 function including the nuclease functions of the SN domains, any potential scaffolding functions, and all Tudor domain and SDMA reader functions. Therefore, these current models are insufficient for establishing the contribution of the SDMA-related reader functions of SND1.

Here we present the development of a *Snd1* Tudor domain mutant (*Snd1 KI*) GEMM alongside an *Snd1 KO* GEMM to tease apart the *in vivo* role of the SND1 Tudor domain. *Snd1 KO* and *Snd1 KI* mice were viable, but with distinct postnatal phenotypes, suggesting that SND1 has Tudor-independent functions. Quantitative PCR analysis of KO and KI liver samples revealed a role for SND1 in regulating the expression of APPs, as previously reported for the KO [29]. These findings supporting a Tudor-dependent function for the transcriptional regulation of APPs. Finally, we have used the carcinogen diethylnitrosamine (DEN), which induces HCC in mice, to show that both *Snd1 KO* and *Snd1 KI* mice are partially protected against tumor development in this context. Thus, DEN-induced HCC implicates the SDMA-reader properties of the SND1 Tudor domain in carcinogenesis. These results support the use of PRMT5 inhibitors, and the development of small molecule inhibitors that target the SND1 Tudor domain, as novel treatments against HCC. The validity of these therapeutic approaches can be addressed in the future using our pre-clinical mouse models.

Results

To address the role of SND1's methylation effector function *in vivo*, we generated a SND1 knockout mouse line that expressed no SND1 (*Snd1 KO*) and a mouse line that expressed normal levels of SND1 that harbored a single mutation in the Tudor domain (*Snd1 KI*).

Generation of the SND1 knockout mouse models

To create the *Snd1 KO* GEMM, we designed a CRISPR/Cas9 guide RNA that targeted the third exon of SND1 and lies within the SN1 domain (Figure 1A). The sgRNA and purified Cas9 protein were micro-injected into 1-cell embryos and transferred into pseudo-pregnant female mice to complete gestation. The resulting pups were genotyped for out-of-frame genetic deletions in this region, which arise though faulty DNA repair. We obtained one *Snd1 KO*, which was subjected to Sanger sequencing to reveal a sequence change starting at amino acid number 91 and introducing a stop codon seven residues down-stream of this position (Figure 1A). The founder was backcrossed onto a FVB background for four generations to minimize the chances of recovering phenotypes related to off-target events. Heterozygous *Snd1 KO* mice were intercrossed, and mouse

Biochemical Journal (2023) **480** 1805–1816
https://doi.org/10.1042/BCJ20230384

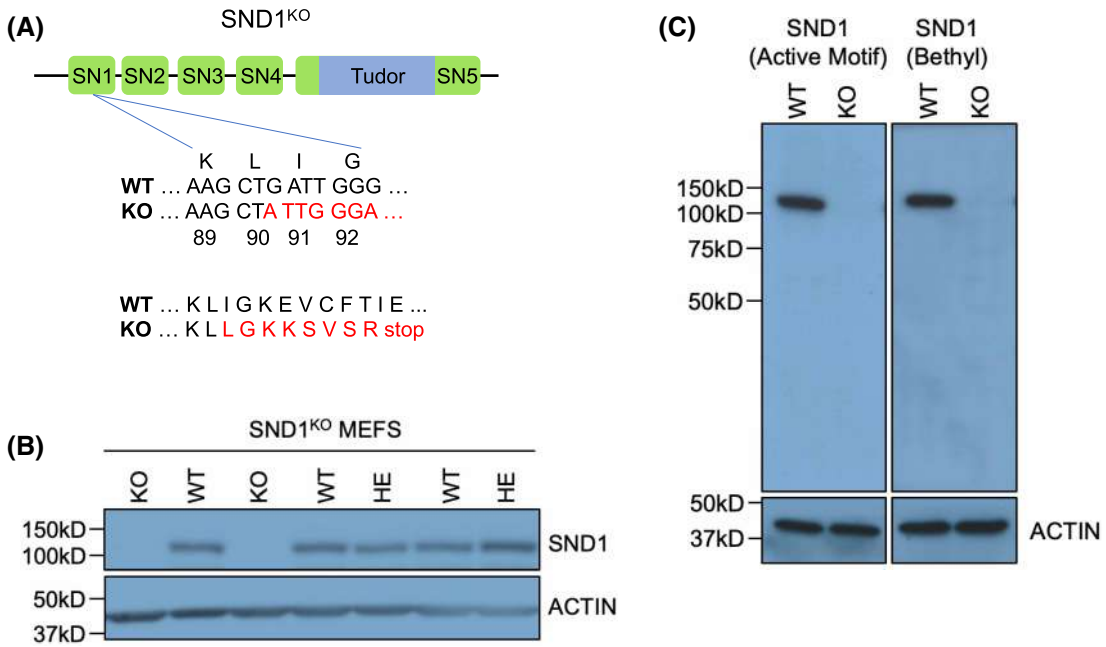

Figure 1. Generation and characterization of SND1 KO mice.

(**A**) *Snd1 KO* mouse design. CRISPR/Cas9 editing resulted in the loss of a single nucleotide (G) in codon 90 causing a frame shift, and introducing a premature stop codon in the third exon, which encodes the first SN-domain. The DNA and amino acid sequence changes are highlighted in red. (**B**) Western blot analysis of protein isolated from MEFs derived from a *Snd1 KO* heterozygous cross. Homozygous null MEFs are indicated as KO, homozygous wild-type as WT and heterozygous MEFs as HE. Top panel shows SND1, bottom panel depicts the β-actin loading control. (**C**) Western blot analysis of protein isolated from immortalized WT and KO MEFs. Two different anti-SND1 antibodies were used, obtained from Active Motif and Bethyl, respectively. Bottom panels depicts the β-actin loading control.

embryonic fibroblasts (MEFs) were generated from 13.5 dpc (days post-coitus) mouse embryos. Western analysis of MEFs isolated from a single litter established that the *Snd1 KO* samples did not express detectable protein (Figure 1B). The epitope that is recognized by this antibody (Active Motif) lies within the SN4 domain. We next generated immortalized MEF WT and KO cell lines. These MEFs were subjected to Western analysis with Active Motif antibody as well as a second antibody raised to the N-terminus of SND1 (Bethyl). Both antibodies did not detect a SND1 protein (Figure 1C), indicating that no SND1 protein is produced in these *Snd1 KO* mice.

Generation of the SND1 knockin mouse models

The structure of the SND1 Tudor domain has been solved with two different arginine methylated peptides, revealing the formation of a four-residue aromatic cage involving F740, Y746, Y763 and Y766 [30]. Mutations in any of these four sites dramatically reduces binding to SDMA-containing peptides [30]. We validated these reported findings by introducing the Y766L mutation into a Tudor-GST fusion and testing it in a peptide-pulldown assay with an SDMA GAR motif (Figure 2A). We also transiently expressed GFP fusions of full-length SND1, WT and Y766L mutant, in 293T cells. These transfected cells were subjected to a co-IP experiment for SmB. The Tudor domain of SND1 has previously been shown to mediate and interaction with arginine methylated Sm proteins, SmB and SmB' [8]. The GFP-SND1 Y766L mutant was unable to co-IP with SmB, but the WT was (Figure 2B).

To generate a genetically modified knockin mouse, we again micro-injected sgRNA and purified Cas9 protein into 1-cell embryos, but this time donor DNA was also added to the mix to facilitate homologs recombination [31], at the codon for the Y766 site. The designed mutation generated a novel *AvrII* restriction enzyme site and was used to identify founders (Figure 2C). The founder was validated by Sanger sequencing and then backcrossed onto a FVB background for four generations to separate potential off-target events.

Biochemical Journal (2023) **480** 1805–1816
https://doi.org/10.1042/BCJ20230384

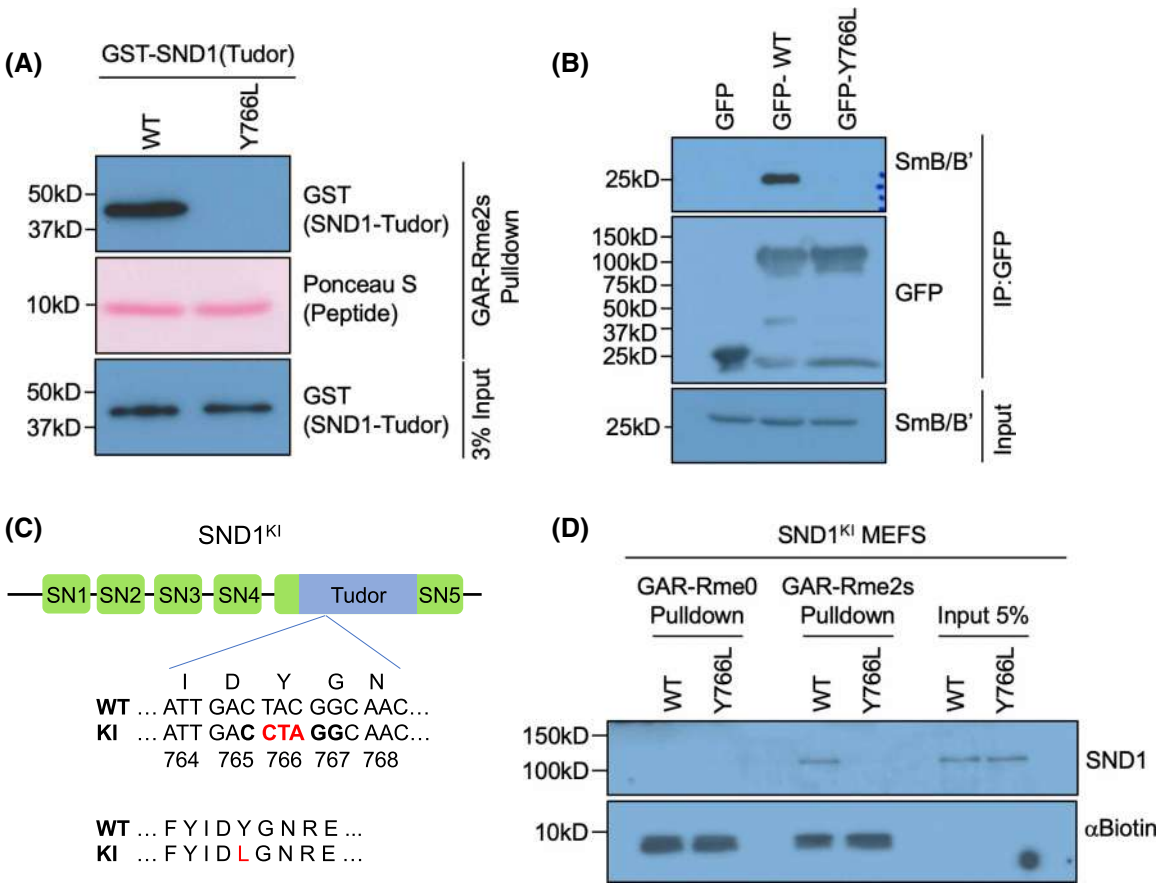

Figure 2. Generation and characterization of SND1 KI mice.

(**A**) Peptide pulldown of recombinant GST-Tudor domain of SND1, wither of *WT* or harboring the Y766L mutation. The pulldown assay was performed using SDMA methylated (Rme2s) biotinylated glycine-arginine-rich (GAR) peptide. Equal peptide loading was validated by Ponceau S staining. (**B**) 293T cells were transiently transfected with GFP, GFP-SND1 (GFP-WT) and GFP-SND1 mutant (GFP-Y766L). Immunoprecipitation was performed with an anti-GFP antibody, and Western analysis was performed for SmB/B' and GFP. (**C**) *Snd1 KI* mouse design. CRISPR/Cas9 editing was used to introduce a CTA codon in place of a TAC codon to create a Y766L substitution as highlighted in red. The nucleotide change generated a *AvrII* restriction enzyme site (CCTAGG in bold) which was used for subsequent genotyping. (**D**) Peptide pulldown from primary MEFs of *WT* and *Snd1 KI* mice (Y766L). Protein extracts from the indicated MEFs were used in a pulldown assay with SDMA methylated (Rme2s) and unmethylated (Rme0) biotinylated glycine-arginine-rich (GAR) peptides. The associated SND1 (upper panel) and the biotinylated peptide loading control were detected by western blot using anti-SND1 (SND1) antibodies and HRP-conjugated streptavidin (αBiotin).

Heterozygous *Snd1 KI* mice were intercrossed, and mouse embryonic fibroblasts (MEFs) were then generated from 13.5 dpc mouse embryos. Protein extracts from *Snd1 WT* and homozygous *Snd1 KI* MEFs were used in pulldown assays with methylated and unmethylated GAR motif peptides. The SDMA-GAR motif could pull-down SND1 from the WT extract but not from the KI extract (Figure 2D), confirming the establishment of a genetically engineered mouse that expresses normal levels of SND1 but cannot read SDMA marks.

Phenotypic comparison of the two SND1 mouse models

When breeding the two mouse lines, we noticed a slight decrease in fertility in the *Snd1 KO* mice. Litter sizes had significantly fewer pups in *Snd1 KO* homozygous crossed mice, while *Snd1 KI* homozygous crossed mice did not have a significant change in litter size compared with *WT* mice (Figure 3A). In keeping with this observation, in both *Drosophila* and mice, SND1 has been implicated in spermatogenesis [29,32]. We also noticed that *Snd1 KO* males were not successful breeders after 4 months of age. Furthermore, following homozygous

Biochemical Journal (2023) **480** 1805–1816
https://doi.org/10.1042/BCJ20230384

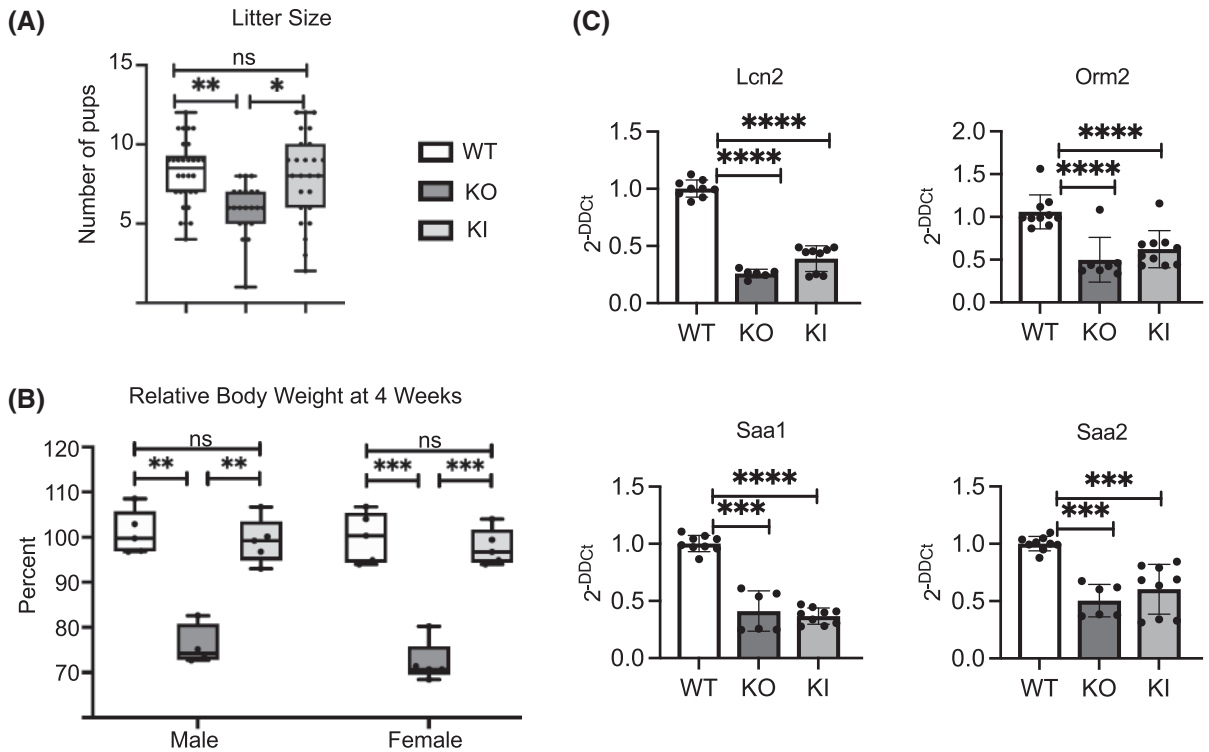

Figure 3. SND1 KO and KI mice are phenotypically distinct but regulate the expression of APP genes similarly.
(**A**) Litter size of *Snd1 KO* and *Snd1 KI* homozygous crossed mice. Points records the number of pups per litter. Pups were counted on the day of birth. $n = 21$, 30 and 25 for WT, KO, and KI, respectively. (**B**) The relative body mass of 4-week-old *Snd1 KO* and *Snd1 KI* mice resulting from heterozygous crosses. $n =$ WT (3m, 5f), KO (3m, 5f) and KI (5m, 5f). (**C**) RT-qPCR of selected acute phase proteins genes, performed in triplicate for 3 WT, 2 KO, and 3 KI independent biological replicates for each genotype. Statistical *t*-test, two-tailed unpaired, *P*-value * $P < 0.5$; ** $P < 0.01$; *** $P < 0.001$; **** $P < 0.0001$.

crosses we observed a decreased mass in both 4-week-old male and female *Snd1 KO* mice (Figure 3B), reflective of other recent reports [29]. One copy of *Snd1* was sufficient to rescue the mass difference. This difference in size was not present in the *Snd1 KI* mice, indicating *Snd1* has a role in development and growth that is unaffected by our Tudor domain mutation.

In mice, *Snd1* overexpression promotes hepatocellular carcinoma (HCC) [22], and *Snd1* was identified as a potential driver of HCC in both *Pten null* and chronic hepatitis B mouse models, via mutagenic Sleeping Beauty transposon screens [20,21]. We sought to determine if loss of SND1 or mutation of the SND1 Tudor domain might influence gene expression that could ultimately impact oncogenic pathways in the liver. *Snd1 KO* gene expression profile was recently performed by the Silvennoinen group [29]. Several of the top down-regulated genes included acute inflammatory response genes (APPs) involved in innate immunity. As chronic inflammation is a known driver of HCC, we tested the RNA level of these genes by qPCR. Lcn2, Orm2, Saa1, and Saa2 were all significantly down-regulated in *Snd1 KO* and *KI* liver samples compared with *WT* (Figure 3C). Importantly, RNA isolated from both the *Snd1 KO* and *KI* liver show similar levels of reduced expression of the APP set we tested. This data indicates that the Tudor domain of SND1 is critical for the normal expression of these APP genes. These genes, which play a major role in innate immunity, are known to be regulated by IL6/STAT3 signaling in the liver. However, lipopolysaccharide (LPS) activation of IL6 is not negatively impacted in *Snd1 KO* bone marrow-derived macrophages [29]. Thus, currently it is unclear how SND1 regulates the expression of acute phase proteins.

Carcinogenic challenge of the SND1 knockout and knockin mice

Three-fold overexpression of SND1 in a GEMM promotes HCC after carcinogenic challenge, resulting in a doubling of liver weight due to the increased tumor burden [22]. Similarly, a two-fold increase in SND1

Biochemical Journal (2023) **480** 1805–1816
https://doi.org/10.1042/BCJ20230384

protein levels were observed in 70% of human HCC samples contained on a tissue microarray [21]. To determine whether either loss of SND1 or mutation of the SND1 Tudor domain might have the opposite effect and be protective against the development of HCC, we treated mice with the carcinogen diethylnitrosomine (DEN).

DEN induces carcinogenic liver injury in mice [33–35]. In cells, DEN is activated by cytochrome P450 enzymes that generate alkylating metabolites which are added to DNA bases. These events trigger DNA damage responses which can result in cell death, proliferative response, and random oncogenic mutations. A single DEN injection in two-week-old pups is sufficient to drive liver carcinogenesis in close to 100% of male mice after 9 months [33], making it useful for comparing liver tumorigenesis in differing genetic conditions. We injected two-week-old male pups with DEN in *Snd1 KO*, *Snd1 KI*, and *WT* control littermates and assessed tumor development at nine months (Figure 4A). All injected mice survived the duration of the experiment. A gross view of representative livers from 9-month-old mice shows more abundant and larger surface nodule development in the WT mice than in either the SND1 KO or SND1 KI mice (Figure 4A).

To compare overall tumor burden and to create a complete picture of the extent of neoplastic growth between *Snd1 KO*, *Snd1 KI*, and *WT* livers, we established a pipeline to assess tumor type, average tumor-foci number, and average tumor area. In brief, we sectioned all five liver lobes from each mouse and performed H&E staining on each section. The stained sections were scanned with an Aperio AT2 slide scanner. Using ImageScope software, the area of each tumor foci and total area of each liver lobe was calculated. The total tumor area was expressed as a ratio of tumor to total section area. The images were then reviewed by a pathologist for the diagnosis of hepatocellular carcinoma, adenoma and hypertrophy (Figure 4B). The proportion of

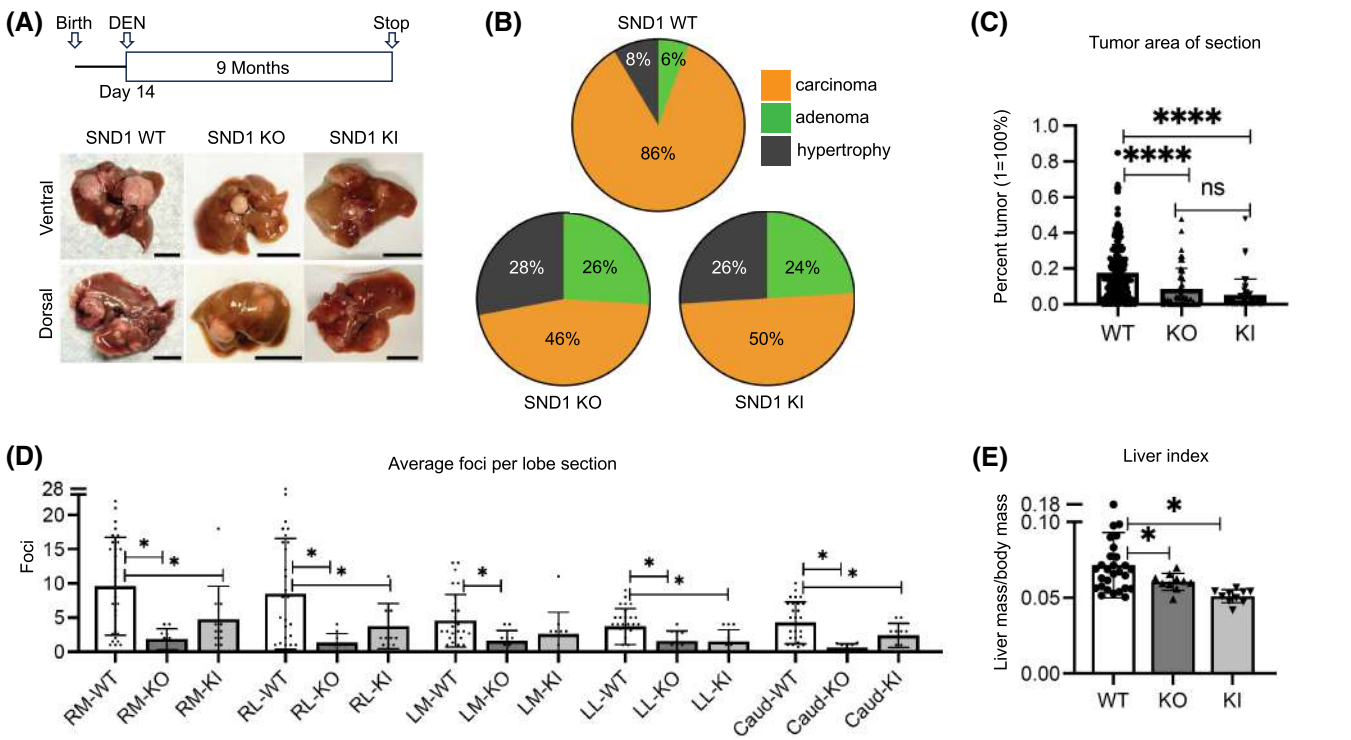

Figure 4. *Snd1* KO and KI is hepatoprotective against DEN-induced HCC.

(**A**) (Top) Schematic of diethylnitrosamine (DEN) injection schedule. Only male mice were used for DEN injection studies. *n* = WT (28); KO (10) and KI (10). All mice survived to nine-month termination. (Bottom) Representative images of whole liver with gallbladder (scale bar = 1 cm). Ventral and dorsal respective to mouse orientation. (**B**) Ratio of observed pathology findings from liver lobe sections representing all 240 lobes from 48 mice (*n* = 50 lobes from each of KO and KI and 140 from WT). Hepatocellular carcinoma and adenocarcinoma were binned together as carcinoma. (**C**) Percent tumor area per total section area of all tumor types from the livers in **B**, obtained using ImageScope and plotted as the ratio of tumor to liver area. (**D**) Number of tumor foci per lobe section from the livers in b. Sections with hepatocellular hypertrophy had no foci. Right medial (RM), right lateral (RL), left medial (LM), left lateral (LL), caudate (Caud). (**E**) Ratio of liver plus gallbladder mass to full mouse from the livers in b. Mouse liver mass was obtained post sacrifice, prior to further manipulation. Statistical *t*-test, two-tailed unpaired, *P*-value * $P < 0.05$; **** $P < 0.0001$.

liver sections with malignant carcinoma was significantly lower in both *Snd1 KO* and *KI* mice when compared with *Snd1 WT* mice (46% and 50% vs. 88%, respectively), which corresponded to a higher proportion of sections with only hepatocellular hypertrophy (28% and 26% vs 8%, respectively) or benign adenoma (26% and 24% vs. 6%, respectively). Moreover, the mean ratio of the combined area of all tumor types to total section area was also significantly decreased in *Snd1 KO* and *KI* mice compared with *WT* controls (Figure 4C). A deeper analysis of individual liver lobes revealed that the mean number of tumor foci was significantly lower in all five lobes derived from *KO* mouse sections, and in four of five lobes of *KI* mouse sections, compared with *WT* (Figure 4D).

We observed that the body weight of one-month-old male and female *Snd1 KO* mice was reduced by roughly 20% (Figure 3B), but at least for DEN-treated mice, this difference in body weight was no longer present at 9 months. It was independently noted that *Snd1 KO* mice have smaller livers at 2 months [29]. Similarly, at 9 months of age, despite whole body mass being similar in treated mice, liver mass was significantly decreased between both *Snd1* mutant lines compared with *WT*. This resulted in the mean liver index being significantly lower in mutant compared with *WT* lines (Figure 4E). Taken together, these results indicate that either the loss of SND1 (KO) or incapacitation of the Tudor domain (KI) confers hepatoprotection against DEN-induced HCC.

Discussion

Structure/function studies of SND1 *in vivo* provide valuable insight into the potential importance of its scaffolding, nuclease, and methyl-reader properties (Figure 3). Much of the previous work on SND1 has focused on the role of the SN-domains and their contribution to SND1 nuclease activity. However, SND1 is a major effector of SDMA marks through its Tudor domain [3]. Here, we provide evidence for Tudor-dependent roles of SND1 in gene expression regulation and in the development of HCC.

RNA expression analysis of SND1 loss-of-function in the liver, shown by us (Figure 3C) and others [29], reveals that the largest effects are seen on genes that encode acute phase proteins (APPs). The acute-phase response is part of a general, systemic response to infections and tissue damage. By definition, proteins whose plasma concentrations change by at least 25% in response to pro-inflammatory stimuli are termed APPs [36]. APPs are produced primarily in the liver and their production is triggered by inflammatory interleukin-6 (IL-6). It is unclear whether the induced APPs are bystanders or participants in carcinogenesis [37]. However, chronic inflammation is a hallmark of HCC formation. If APPs are indeed participants in the development of HCC, then their reduced expression in *Snd1 KO* and *KI* livers might be responsible for the hepato-protective effect we observe after DEN-treatment.

In human HCC the most frequent genetic alterations are *TERT* promoter amplification, *TP53* mutation or deletion, and *CTNNB1* or *ARID2* mutation [38]. Remaining recurrent genetic aberrations make up <10% of clinical cases each. It is generally thought that ethnicity, etiology, and environmental exposure all contribute to this confounding heterogeneity in HCC. Adding to this complexity, the liver exhibits inter- and intra-lobular heterogeneity in gene expression profiles further confounding genetic considerations alone [39]. Given the highly heterogeneous genomic landscape of HCC [38,40,41], we deemed that DEN-induced HCC would provide a valuable proof of principle demonstrating a potential vulnerability of HCC to loss of SND1 function. We found that the loss of either SND1 or its Tudor domain reader function has a protective role in DEN-induced tumorigenesis (Figure 4). Furthermore, this work indicates that the Tudor domain may provide a novel druggable target for the treatment of HCC.

The methylarginine reader function of SND1 can be therapeutically targeted in two ways; (1) either limiting the available SDMA marks recognized by the SND1 Tudor domain by inhibiting the protein arginine methyltransferase that deposits SDMA (i.e. using PRMT5 inhibitors), or (2) developing small molecule inhibitors that dock into the aromatic cage of the SND1 Tudor domain to block interaction of this domain with SDMA. A large number of PRMT5 inhibitors have been developed [42]; however, PRMT5 has many substrates and is often essential for cell viability. Thus, a therapeutic window may be difficult to achieve. Importantly, copy number alteration analysis has identified a recurrent homozygous deletion of CDKN2A and MTAP in HCC primary tumors [43], which would make this HCC-subset selectively sensitive to second-generation PRMT5 inhibitors that are MTA-dependent. Alternatively, inhibitors could be developed that block the ability of the SND1 Tudor domain to read SDMA marks. Notably, SMN and SMNDC1 are two related readers of PRMT5-catalyzed SDMA marks and inhibitors that block these Tudor/SDMA interactions have recently been described [44,45], setting a precedent for successfully adopting this approach. Importantly, the SMN Tudor

Biochemical Journal (2023) 480 1805–1816
https://doi.org/10.1042/BCJ20230384

domain small molecule inhibitor does not bind the Tudor domain of SND1 [44], raising the possibility that the reverse is also possible and that SND1 inhibitors can be identified that do not block SMN-dependent protein–protein interactions.

Experimental procedures

Generation of mouse models

Both *Snd1 KO* and *KI* mice were generated using CRISPR/Cas9 gene-editing technology. sgRNA, donor DNA, and Cas9 protein were from Horizon Discovery. *Snd1 KI* mice were generated using sgRNA targeting tyrosine 766 of *Snd1*, donor DNA encoding the tyrosine to leucine substitution (Y-to-L mutation) were designed by Horizon Discovery. An *AvrII* restriction site was also introduced into the donor DNA for easy genotyping. To generate the *Snd1 KO* and *KI* mice, the sgRNA, Cas9 protein, and donor DNA (for *Snd1 KI* mice generation) were micro-injected into 1-cell FVB embryos. The injected embryos were transferred into pseudo-pregnant recipient female mice. Genomic DNA from the resultant pups was isolated and used for PCR genotyping. PCR products were purified and sequenced to identify heterozygous mice as founders. The founders were back-crossed with FVB strain background mice for four generations to separate any potential off-target event. The sequences of sgRNAs and donor DNA are as follows:

Snd1-KO sgRNA: tccttcgcaagaagctgattGGG; *Snd1-KI* sgRNA: catgtcttctacatcgactaCGG

Snd1-KI donor DNA: CATTGCAGGTACCGCGCCCGGGTAGAAAAGGTGGAGTCCCCTGCCAAAGT GCATGTCTTCTACATCGACCTAGGCAACGTGAGTGCTGGGACCAGGGTGGAAAACAGGCAAGGCAGG-GACCATTGGGCACAG

Mouse genotyping

Snd1 KO mice were genotyped as previously described [46]. In brief, genomic DNA extracted from pup tail clips and used as template for amplification of the target gene region by PCR, to yield a 456 bp PCR product. The PCR product was split into two aliquots, and a *Snd1 wild-type (WT)* control PCR product was added to one of the two aliquots. The PCR products were denatured and annealed before digestion with T7E1 endo-nuclease. The digested materials were then separated by electrophoresis through a 2% agarose gel. In the absence of an added *Snd1 WT* control PCR product, only the heterozygous PCR samples were efficiently cleaved by T7E1, resulting in smaller cleaved products (228 bp/227 bp); in the presence of the added *Snd1 WT* control PCR products, the *Snd1 KO* samples are separated from the *Snd1 WT* samples, as the added *Snd1 WT* control PCR products resulted in the formation of heteroduplexes with the *Snd1 KO* samples that are sensitive to cleavage by T7E1.

Snd1-KO genotyping forward primer: TTTAGGAGGCCCTGAGTGTG

Snd1-KO genotyping reverse primer: CAGGGCTGCTAGAGGTATGC

Snd1 KI mice were genotyped using genomic DNA extracted from either tail clips from pups or extracted tissues and subjected to amplification by PCR using the primers described below for 28 cycles. Amplicons were digested overnight with *AvrII* (New England Biolabs) using their recommended protocol and were visualized following electrophoresis through a 2% agarose gel. Digested PCR products from homozygous *KI* mice resulted in two bands (261 bp/145 bp), whereas products from heterozygous *KI* mice displayed three bands (406 bp/261 bp/145 bp), representing *WT* and *KI* alleles.

Snd1-KI genotyping forward primer: TATTAATCTGCTGCCCGTGCT

Snd1-KI genotyping reverse primer: GAAGAGTGGCGGTGACCAATA

Peptide pulldown assay

Streptavidin beads (Millipore, Cat# 16-126) were pre-washed with cell lysis buffer before incubation with biotinylated GAR-un/Rme2s peptides (10 μg) in 500 μl cell lysis buffer for 1 h at 4°C with rocking for conjugation. Lysis buffer was composed of the following Sigma compounds: 50 mM sodium diphosphate (Cat# S0751-100G), 300 mM sodium chloride (Cat# S9888-25G), 10 mM imidazole (Cat# I5513-25G) all adjusted to pH 8.0. The conjugated peptide-beads complex was then incubated with cell lysates prepared from primary MEFs for 1 h at 4°C with rocking. After incubation, the bound proteins were eluted by addition of SDS-Lammeli buffer for western blot analysis. GAR peptide sequences are as follows with SDMA marked by '*':

GAR-un peptide: GGRGRGGGFRGRGRGGGG-BIOTIN

GAR-Rme2s peptide: GG[R**]G[R**]GGGF[R**]G[R**]G[R**]GGGG-BIOTIN

Immunoblot analysis

This study used the following antibodies: SND1, Active Motif (Cat# 61473); SND1, Bethyl (Cat# A302-883A); β-actin, Sigma (Cat# A1978); Streptavidin-HRP, Pierce (Cat# 21126), anti-rabbit IgG HRP secondary, Cell Signaling Technology (Cat# 7074), ECL anti-mouse IgG HRP, GE Healthcare (Cat# NXA931). The following was used for western blotting: Equivalent concentrations of protein were boiled in 1× SDS Laemmli buffer for 10 min. Boiled samples were loaded into 10–15% in-house prepared gradient polyacrylamide gels. Gels were made with: 30% Acrylamide bis (Bio-Rad, Cat# 1610158), 1:1 diluted SDS solution 20% (Bio-Rad, Cat# 1610418), N,N,N′,N′ tetramethyl ethylenediamine (Acros Organics, Cat#420580050), and ammonium persulfate (Sigma, Cat# A3678-100G). Proteins were transferred to a methanol activated 0.45 μm PVDF membrane (Millipore, Cat# 88518) using semi-wet transfer. Wash buffer contained 1× PBS with 0.5% Tween20 (Bio-Rad, Cat# 1610781) (PBS-T), and blocking buffer contained 5% nonfat power milk (LabScientific, Cat# M0841) dissolved in PBS-T (5% milk). PVDF membranes from semi-wet transfers were blocked for 1 h in 5% milk followed by incubating overnight in 5% milk with the primary antibody. This was followed by three 10 min washes in 1× PBS-T. The secondary antibody in 5% milk was added for 1 h rocking at RT followed by three PBS-T washes at 10 min each. Membranes were developed using Western Lightning (PerkinElmer, NEL103E001EA).

Mouse experiments

All mice used for experiments were age and sex matched as indicated in the text. The mouse experimental protocol was reviewed and approved by the Institutional Animal Care and Use Committee at MD Anderson Cancer Center (ACUF# 00001090-RN03). All mice were housed, and animal experiments performed at the MD Anderson Cancer Center Research Animal Support Facility — Houston. Anesthesia was not used in mouse experiments. Mice were killed using compressed CO_2 at a 50% per minute displacement rate until loss of consciousness plus 2 min, followed by cervical dislocation.

DEN injection models

DEN (Sigma, N0258-1G), also known as N-nitrosodiethylamine, was diluted to 2 mg/ml in sterile 0.9% saline and stored at 4°C. All DEN injections were performed on 14-day old male mice. Pups were interperitoneally injected with 20 mg/kg DEN using a 1 ml TB/insulin style syringe and moved into a fresh Innovive cage for 14 days post injection to allow wash out, switching the cage and weaning at 7 days post injection. Mature mice were then moved into normal caging and allowed to grow tumors for 272–274 days. We excluded females from DEN studies as they develop HCC in <30% of DEN injections with varied penetrance [33]. This is compared with nearly 100% penetrance in males. Increased HCC incidence in males is also seen in humans. Thus, DEN induced HCC is a non-optimal approach for directly comparing tumorigenesis in females but is excellent for foundational HCC studies in males.

RT-qPCR analysis

RNA was harvested for qPCR experiments. Total RNA was harvested from 2-month-old male mice using manufacturer recommendations using TRIzol reagent (Ambion, Cat# 15596026) and precipitated in isopropanol an additional time to increase purity of total RNA. A cDNA library was generated with an iScript cDNA Synthesis Kit (Bio-Rad, Cat# 1708891) using the manufacturer's recommended volumes and thermocycler conditions, before dilution in nuclease free water. From the diluted library, 20 ng cDNA was added to 500 nM primers in recommended volumes of 1× iTaq Universal SYBR Green Supermix (Bio-Rad, Cat# 1725122) in 384 well plates. Thermocycler conditions were: step 1 — 95°C for 5 min; step 2 — 95°C for 15 s, 60°C for 1 min; repeat step 2 39×; step 3 — 65°C for 5 s, and 95°C 50 s. Expression change was calculated using ΔΔCt methodology. Expressly, Ct values of *Gapdh* were obtained for each biological replicate. The ΔCt was next calculated as the difference of each raw Ct value from the respective biological housekeeping gene average. The average ΔCt was obtained for only the biological WT control for each gene of interest. The ΔΔCt was then calculated as the difference between each ΔCt, and the average ΔCt of the biological WT control. We then calculated and reported $2^{-\Delta\Delta Ct}$.

Primers were designed using the NIH Primer BLAST software. Primers were chosen based on criteria of having similar size, Tm, covering splicing junction sites, and low probability predictions for off-target amplification.

Biochemical Journal (2023) **480** 1805–1816
https://doi.org/10.1042/BCJ20230384

Saa1 F: CATTTGTTCACGAGGCTTTCC; Saa1 R: CTGAGTTTTTCCAGTTAGC
Saa2 F: CATTTATTGGGGAGGCTTTCC; Saa2 R: CTCCATCTTTCCAGCCAGC
Lcn2 F: TGAAGGAACGTTTCACCCGC; Lcn2 R: CCATTGGGTCTCTGCGCATC
Orm2 F: CGCTGTTGGAAGCTCAGAACC; Orm2 R: TAGGACAGCCGCACCAATGA

Data Availability

This manuscript does not contain any mass spec data or genomic data. We will provide the two mouse models generated in this study to anyone who requests them. The sharing of these GEMMs will require an MTA with MD Anderson Cancer Center.

Competing Interests

Mark T. Bedford is the co-founder of EpiCypher.

Funding

This work was supported in part by grants from the NIH to M.T.B. (GM126421), D.G.J. (CA214723), and by the MD Anderson Cancer Center SPORE in Hepatocellular Carcinoma Grant P50 CA217674.

Open Access

Open access for this article was enabled by the participation of University of Texas MD Anderson Cancer Center in an all-inclusive Read & Publish agreement with Portland Press and the Biochemical Society under a transformative agreement with EBSCO.

CRediT Author Contribution

Mark T. Bedford: Conceptualization, Funding acquisition, Writing — original draft, Project administration. **Tanner Wright:** Conceptualization, Formal analysis, Validation, Methodology, Writing — original draft. **Yalong Wang:** Conceptualization, Formal analysis, Methodology, Writing — review and editing. **Sabrina A. Stratton:** Methodology. **Manu Sebastian:** Methodology. **Bin Liu:** Methodology. **David G. Johnson:** Conceptualization, Resources, Funding acquisition.

Acknowledgements

We would further like to thank the DVMS Clinical Pathology Core, DVMS Anatomical Pathology Core, and the Smithville Histology Core for their assistance with necropsies and histological staining. We thank Briana Dennehey for proofreading and edits and helpful comments.

Abbreviations

ADMA, asymmetric dimethylarginine; DEN, diethylnitrosamine; EBNA-2, Epstein–Barr virus nuclear antigen 2; GAR, glycine-arginine-rich; HCC, hepatocellular carcinoma; MEFs, mouse embryonic fibroblasts; MMA, monomethylarginine; PRMT5, protein arginine methyltransferase 5; PRMTs, protein arginine methyltransferases; PTM, posttranslational modification; SDMA, symmetric dimethylarginine; *Snd1 KO*, *Snd1* knockout; SND1, Staphylococcal nuclease Tudor domain containing 1; STAT5, signal transducer and activator of transcription 5; STAT6, signal transducer and activator of transcription 6.

References

1 Blanc, R.S. and Richard, S. (2017) Arginine methylation: the coming of age. *Mol. Cell* **65**, 8–24 https://doi.org/10.1016/j.molcel.2016.11.003
2 Bedford, M.T. and Clarke, S.G. (2009) Protein arginine methylation in mammals: who, what, and why. *Mol. Cell* **33**, 1–13 https://doi.org/10.1016/j.molcel.2008.12.013
3 Wang, Y. and Bedford, M.T. (2023) Effectors and effects of arginine methylation. *Biochem. Soc. Trans.* **51**, 725–734 https://doi.org/10.1042/BST20221147
4 Ochoa, B., Chico, Y. and Martinez, M.J. (2018) Insights into SND1 oncogene promoter regulation. *Front. Oncol.* **8**, 606 https://doi.org/10.3389/fonc.2018.00606
5 Wright, T., Wang, Y. and Bedford, M.T. (2021) The role of the PRMT5–SND1 axis in hepatocellular carcinoma. *Epigenomes* **5**, 2 https://doi.org/10.3390/epigenomes5010002
6 Chen, C., Jin, J., James, D.A., Adams-Cioaba, M.A., Park, J.G., Guo, Y. et al. (2009) Mouse Piwi interactome identifies binding mechanism of Tdrkh Tudor domain to arginine methylated Miwi. *Proc. Natl Acad. Sci. U.S.A.* **106**, 20336–20341 https://doi.org/10.1073/pnas.0911640106
7 Friberg, A., Corsini, L., Mourao, A. and Sattler, M. (2009) Structure and ligand binding of the extended Tudor domain of D. melanogaster Tudor-SN. *J. Mol. Biol.* **387**, 921–934 https://doi.org/10.1016/j.jmb.2009.02.018

8 Gao, X., Zhao, X., Zhu, Y., He, J., Shao, J., Su, C. et al. (2012) Tudor staphylococcal nuclease (Tudor-SN) participates in small ribonucleoprotein (snRNP) assembly via interacting with symmetrically dimethylated Sm proteins. *J. Biol. Chem.* **287**, 18130–18141 https://doi.org/10.1074/jbc.M111.311852
9 Cappellari, M., Bielli, P., Paronetto, M.P., Ciccosanti, F., Fimia, G.M., Saarikettu, J. et al. (2014) The transcriptional co-activator SND1 is a novel regulator of alternative splicing in prostate cancer cells. *Oncogene* **33**, 3794–3802 https://doi.org/10.1038/onc.2013.360
10 Zheng, S., Moehlenbrink, J., Lu, Y.C., Zalmas, L.P., Sagum, C.A., Carr, S. et al. (2013) Arginine methylation-dependent reader-writer interplay governs growth control by E2F-1. *Mol. Cell* **52**, 37–51 https://doi.org/10.1016/j.molcel.2013.08.039
11 Roworth, A.P., Carr, S.M., Liu, G., Barczak, W., Miller, R.L., Munro, S. et al. (2019) Arginine methylation expands the regulatory mechanisms and extends the genomic landscape under E2F control. *Sci. Adv.* **5**, eaaw4640 https://doi.org/10.1126/sciadv.aaw4640
12 Callebaut, I. and Mornon, J.P. (1997) The human EBNA-2 coactivator p100: multidomain organization and relationship to the staphylococcal nuclease fold and to the tudor protein involved in Drosophila melanogaster development. *Biochem. J.* **321**, 125–132 https://doi.org/10.1042/BJ3210125
13 Paukku, K., Yang, J. and Silvennoinen, O. (2003) Tudor and nuclease-like domains containing protein p100 function as coactivators for signal transducer and activator of transcription 5. *Mol. Endocrinol. (Baltimore, Md.)* **17**, 1805–1814 https://doi.org/10.1210/ME.2002-0256
14 Yang, J., Aittomäki, S., Pesu, M., Carter, K., Saarinen, J., Kalkkinen, N. et al. (2002) Identification of p100 as a coactivator for STAT6 that bridges STAT6 with RNA polymerase II. *EMBO J.* **21**, 4950–4958 https://doi.org/10.1093/EMBOJ/CDF463
15 Hu, P., Zhao, H., Zhu, P., Xiao, Y., Miao, W., Wang, Y. et al. (2019) Dual regulation of Arabidopsis AGO2 by arginine methylation. *Nat. Commun.* **10**, 844 https://doi.org/10.1038/s41467-019-08787-w
16 Jariwala, N., Rajasekaran, D., Srivastava, J., Gredler, R., Akiel, M.A., Robertson, C.L. et al. (2015) Role of the staphylococcal nuclease and tudor domain containing 1 in oncogenesis (review). *Int. J. Oncol.* **46**, 465–473 https://doi.org/10.3892/IJO.2014.2766
17 Chidambaranathan-Reghupaty, S., Mendoza, R., Fisher, P.B. and Sarkar, D. (2018) The multifaceted oncogene SND1 in cancer: focus on hepatocellular carcinoma. *Hepatoma Res.* **4**, 32–32 https://doi.org/10.20517/2394-5079.2018.34
18 Cui, X., Zhang, X., Liu, M., Zhao, C., Zhang, N., Ren, Y. et al. (2020) A pan-cancer analysis of the oncogenic role of staphylococcal nuclease domain-containing protein 1 (SND1) in human tumors. *Genomics* **112**, 3958–3967 https://doi.org/10.1016/J.YGENO.2020.06.044
19 Yoo, B.K., Santhekadur, P.K., Gredler, R., Chen, D., Emdad, L., Bhutia, S. et al. (2011) Increased RNA-induced silencing complex (RISC) activity contributes to hepatocellular carcinoma. *Hepatology* **53**, 1538–1548 https://doi.org/10.1002/hep.24216
20 Kodama, T., Yi, J., Newberg, J.Y., Tien, J.C., Wu, H., Finegold, M.J. et al. (2018) Molecular profiling of nonalcoholic fatty liver diseaseassociated hepatocellular carcinoma using SB transposon mutagenesis. *Proc. Natl Acad. Sci. U.S.A.* **115**, E10417–E10426 https://doi.org/10.1073/pnas.1808968115
21 Bard-Chapeau, E.A., Nguyen, A.T., Rust, A.G., Sayadi, A., Lee, P., Chua, B.Q. et al. (2014) Transposon mutagenesis identifies genes driving hepatocellular carcinoma in a chronic hepatitis B mouse model. *Nat. Genet.* **46**, 24–32 https://doi.org/10.1038/ng.2847
22 Jariwala, N., Rajasekaran, D., Mendoza, R.G., Shen, X.N., Siddiq, A., Akiel, M.A. et al. (2017) Oncogenic role of SND1 in development and progression of hepatocellular carcinoma. *Cancer Res.* **77**, 3306–3316 https://doi.org/10.1158/0008-5472.CAN-17-0298
23 Jarrold, J. and Davies, C.C. (2019) PRMTs and arginine methylation: cancer's best-kept secret? *Trends Mol. Med.* **25**, 993–1009 https://doi.org/10.1016/j.molmed.2019.05.007
24 Stopa, N., Krebs, J.E. and Shechter, D. (2015) The PRMT5 arginine methyltransferase: many roles in development, cancer and beyond. *Cell. Mol. Life Sci.* **72**, 2041–2059 https://doi.org/10.1007/s00018-015-1847-9
25 Yang, Y. and Bedford, M.T. (2013) Protein arginine methyltransferases and cancer. *Nat. Rev. Cancer* **13**, 37–50 https://doi.org/10.1038/nrc3409
26 Fu, S., Zheng, Q., Zhang, D., Lin, C., Ouyang, L., Zhang, J. et al. (2022) Medicinal chemistry strategies targeting PRMT5 for cancer therapy. *Eur. J. Med. Chem.* **244**, 114842 https://doi.org/10.1016/j.ejmech.2022.114842
27 Gao, J., Yang, J., Xue, S., Ding, H., Lin, H. and Luo, C. (2023) A patent review of PRMT5 inhibitors to treat cancer (2018 - present). *Expert Opin. Ther. Pat.* **33**, 265–292 https://doi.org/10.1080/13543776.2023.2201436
28 Wang, X., Zhang, C., Wang, S., Rashu, R., Thomas, R., Yang, J. et al. (2021) SND1 promotes Th1/17 immunity against chlamydial lung infection through enhancing dendritic cell function. *PLoS Pathog.* **17**, e1009295 https://doi.org/10.1371/JOURNAL.PPAT.1009295
29 Saarikettu, J., Lehmusvaara, S., Pesu, M., Junttila, I., Partanen, J., Sipilä, P. et al. (2023) The RNA-binding protein Snd1/Tudor-SN regulates hypoxia-responsive gene expression. *FASEB Bioadv.* **5**, 183–198 https://doi.org/10.1096/FBA.2022-00115
30 Liu, K., Chen, C., Guo, Y., Lam, R., Bian, C., Xu, C. et al. (2010) Structural basis for recognition of arginine methylated Piwi proteins by the extended Tudor domain. *Proc. Natl Acad. Sci. U.S.A.* **107**, 18398–18403 https://doi.org/10.1073/PNAS.1013106107
31 Hall, B., Cho, A., Limaye, A., Cho, K., Khillan, J. and Kulkarni, A.B. (2018) Genome editing in mice using CRISPR/Cas9 technology. *Curr. Protoc. Cell Biol.* **81**, e57 https://doi.org/10.1002/cpcb.57
32 Ku, H.Y., Gangaraju, V.K., Qi, H., Liu, N. and Lin, H. (2016) Tudor-SN interacts with Piwi antagonistically in regulating spermatogenesis but synergistically in silencing transposons in Drosophila. *PLoS Genet.* **12**, e1005813 https://doi.org/10.1371/JOURNAL.PGEN.1005813
33 Schulien, I. and Hasselblatt, P. (2021) Diethylnitrosamine-induced liver tumorigenesis in mice. *Methods Cell Biol.* **163**, 137–152 https://doi.org/10.1016/BS.MCB.2020.08.006
34 Tolba, R., Kraus, T., Liedtke, C., Schwarz, M. and Weiskirchen, R. (2015) Diethylnitrosamine (DEN)-induced carcinogenic liver injury in mice. *Lab. Anim.* **49**, 59–69 https://doi.org/10.1177/0023677215570086
35 Swenberg, J.A., Hoel, D.G. and Magee, P.N. (1991) Mechanistic and statistical insight into the large carcinogenesis bioassays on N-nitrosodiethylamine and N-nitrosodimethylamine. *Cancer Res.* **51**, 6409–6414
36 Gabay, C. and Kushner, I. (1999) Acute-phase proteins and other systemic responses to inflammation. *N. Engl. J. Med.* **340**, 448–454 https://doi.org/10.1056/NEJM199902113400607
37 Dempsey, E. and Rudd, P.M. (2012) Acute phase glycoproteins: bystanders or participants in carcinogenesis? *Ann. N. Y. Acad. Sci.* **1253**, 122–132 https://doi.org/10.1111/j.1749-6632.2011.06420.x
38 Llovet, J.M., Zucman-Rossi, J., Pikarsky, E., Sangro, B., Schwartz, M., Sherman, M. et al. (2016) Hepatocellular carcinoma. *Nat. Rev. Dis. Primers* **2**, 16018 https://doi.org/10.1038/NRDP.2016.18
39 Wang, J., Kaur, S., Westermeier, F., Porat-Shliom, N. and Cunningham, R.P. (2021) Liver zonation: revisiting old questions with new technologies. *Front. Physiol.* **12**, 732929 https://doi.org/10.3389/fphys.2021.732929

Biochemical Journal (2023) **480** 1805–1816
https://doi.org/10.1042/BCJ20230384

40 Zhang, Q., Lou, Y., Bai, X.L. and Liang, T.B. (2020) Intratumoral heterogeneity of hepatocellular carcinoma: from single-cell to population-based studies. *World J. Gastroenterol.* **26**, 3720–3720 https://doi.org/10.3748/WJG.V26.I26.3720
41 Llovet, J.M., Kelley, R.K., Villanueva, A., Singal, A.G., Pikarsky, E., Roayaie, S. et al. (2021) Hepatocellular carcinoma. *Nat. Rev. Dis. Primers* **7**, 1–28 https://doi.org/10.1038/s41572-020-00240-3
42 Zheng, J., Li, B., Wu, Y., Wu, X. and Wang, Y. (2023) Targeting arginine methyltransferase PRMT5 for cancer therapy: updated progress and novel strategies. *J. Med. Chem.* **66**, 8407–8427 https://doi.org/10.1021/acs.jmedchem.3c00250
43 Caruso, S., Calatayud, A.L., Pilet, J., La Bella, T., Rekik, S., Imbeaud, S. et al. (2019) Analysis of liver cancer cell lines identifies agents with likely efficacy against hepatocellular carcinoma and markers of response. *Gastroenterology* **157**, 760–776 https://doi.org/10.1053/j.gastro.2019.05.001
44 Liu, Y., Iqbal, A., Li, W., Ni, Z., Wang, Y., Ramprasad, J. et al. (2022) A small molecule antagonist of SMN disrupts the interaction between SMN and RNAP II. *Nat. Commun.* **13**, 5453 https://doi.org/10.1038/s41467-022-33229-5
45 Enders, L., Siklos, M., Borggrafe, J., Gaussmann, S., Koren, A., Malik, M. et al. (2023) Pharmacological perturbation of the phase-separating protein SMNDC1. *Nat. Commun.* **14**, 4504 https://doi.org/10.1038/s41467-023-40124-0
46 Zheng, L., Hill, J., Zheng, L., Rumi, M.A.K. and Zheng, X.L. (2022) A simple, robust, and cost-effective method for genotyping small-scale mutations. *J. Clin. Transl. Pathol.* **2**, 108–115 https://doi.org/10.14218/JCTP.2022.00014